Estimating CO$_2$ emissions from point sources: a case study of an isolated power station

S. R. Utembe[1]**, N. Jones**[2]**, P. J. Rayner**[1]**, I. Genkova**[1]**, D. W. T. Griffith**[2]**, D. M. O'Brien**[3]**,
C. Lunney**[4]**, and A. J. Clark**[4]

[1]University of Melbourne, School of Earth Sciences, Melbourne, Australia
[2]University of Wollongong, Wollongong, Australia
[3]Greenhouse Gas Monitor Australia Pty Ltd, Melbourne, Australia
[4]Vipac Engineers and Scientists, Adelaide, SA, Australia

Correspondence to: S. R. Utembe (steven.utembe@unimelb.edu.au)

Abstract

A methodology to estimate CO_2 emissions from an isolated power plant is presented and illustrated for the Northern Power Station at Port Augusta, South Australia. The method involves measurement of in-situ and column-averaged CO_2 at a site near the power plant, forward modelling (using WRF-Chem) of the observed signals and inverse modelling to obtain an estimate of the fluxes from the power plant. By subtracting the simulated background CO_2 (obtained from Monitoring Atmospheric Composition and Climate CO_2 fields) from the observed and simulated signals, we are able to account for fluxes from the power plant that are mainly responsible for the variations in the CO_2 concentrations. Although the enhancements of the surface concentration of CO_2 are a factor of 10 larger than the enhancements in the column-averaged concentration, the forward transport model has difficulty predicting the in-situ data, which is complicated by sea breeze effects and influence from other local sources. Better simulation is obtained for the column-averaged data leading to better estimates of fluxes. The ratio of our estimated emissions to the reported values is 1.06 ± 0.54. Modelling local biospheric fluxes makes little difference either to the estimated emissions or quality of the fit to the data. Variations in the large-scale concentration field have a larger impact highlighting the importance of good boundary conditions even in the relatively homogeneous Southern Hemisphere. The estimates are insensitive to details of the calculation such as stack height or modelling of plume injection. ~~We conclude~~ Large uncertainties arise from the short duration of the campaign. The results suggest that column-integrated measurements offer a ~~reasonable trade-off between sensitivity and model capability for estimating~~ promising approach to inferring isolated point sources.

1 Introduction

It is widely acknowledged that CO_2 emissions contribute to global climate change (IPCC , 2007). Coal-fired power plants are among the major emitters of CO_2, and with current world reserves of coal being estimated at 930 Gt coal (Shindell and Faluvegi, 2010), it is expected

that emissions of CO_2 from fossil fuels will continue for many decades to come. The Kyoto protocol mandates all participating countries to report their CO_2 emissions (http://unfccc.int/kyoto_protocol/items/2830.php). However, many estimates of CO_2 emissions use bottom-up methods based on plant fuel efficiency, amount of fuel consumed and CO_2 conversion factors rather than direct measurement of CO_2 emissions. These methods may be subject to large uncertainties (Andres et al., 2012). Therefore, there is a need for independent methods to verify emissions. Atmospheric inversions provide one such method.

Atmospheric inversions combine concentration measurements, atmospheric transport models and a statistical estimation procedure (see Enting, 2002; Ciais et al., 2010, for the general principles). Concentration measurements are of two forms, either in-situ or remotely-sensed. These measurements have different uncertainties and sampling characteristics. They thus play complementary roles at different scales.

These complementary scales address different science and policy needs. Atmospheric measurements of the carbon cycle have traditionally addressed large-scale but diffuse processes such as terrestrial or ocean uptake (e.g. Rayner et al., 2008; Basu et al., 2013; Peylin et al., 2013). Rayner and O'Brien (2001) and many subsequent studies showed that the large footprint and coverage of spaceborne column-integrated measurements made them particularly suitable for this task. Hungershoefer et al. (2010), however, showed that this style of measurement might not be optimal for constraining the fossil fuel emissions from a region. The extreme heterogeneity of fossil fuel emissions (Rayner et al., 2010; Asefi-Najafabady et al., 2014) suggests a more targeted approach in which intense and uncertain sources are subject to local measurement. The optimal strategy for such measurements is not clear, but fortunately there is a range of sources with known emissions where we can test approaches.

Remotely-sensed measurements can be further differentiated into ground-based (e.g. Wunch et al., 2011a), airborne (e.g. Abshire et al., 2013) or spaceborne (e.g. Kuze et al., 2009). The Total Carbon Column Observing Network (TCCON) provides precise, continuous measurements of column-averaged abundances of CO_2 during periods of direct solar radiation at the sensor (e.g. Toon et al., 2009; Wunch et al., 2011a). The cost and logistical

requirements of TCCON instruments limit the size of this network. Thus, there is need for the development of low-cost, robust and portable instrumentation to augment the network.

To this end, recently a range of low-cost and portable instruments has been developed such as the $0.16\,\mathrm{cm}^{-1}$ resolution fiber Fabry–Perot interferometer by Kobayashi et al. (2010) and and several low resolution Fourier Transform spectrometers (e.g. Chen et al., 2012; Jones et al., 2012; Gisi et al., 2012; Petri et al., 2012). In this paper we present results from the Greenhouse Gas Monitor Project. [1]

Using a low-cost, low resolution instrument (a modified Bruker IR-Cube) from the same family as the TCCON instrument, we can test whether we observe and model changes in column-averaged CO_2 (hereafter X_{CO_2}) and attribute these accurately to emissions from an isolated power station. In-situ measurements of CO_2 were also made upwind and downwind of the power station together with the column-integrated measurements, and both are used in this study to assess their applicability to estimating fluxes from point sources.

The outline of the paper is as follows. In Sect. 2, a description of the measurement site and instrumentation is presented. This is followed by description of the atmospheric forward transport model and a consideration of the potential sources of CO_2 emissions in the model domain (Sect. 3). Section 4 presents the in-situ and column-averaged data measured during the field trial, which is followed by modelling results of the same (Sect. 5). The methodology for estimating emissions is presented in Sect. 6, followed by a broader discussion of the study's results (Sect. 7). Finally, Sect. 8 summarizes the main findings.

---

2 Sites and instrumentation

2.1 Measurement sites

The trial was conducted from 7 to 16 May 2012 at Port Augusta, South Australia. This location was chosen because it is relatively isolated from major cities (the nearest major city being Adelaide about 290 km to the south) and because of the presence of the coal-fired Northern Power Station (henceforth referred to as NPS), a large emitter of CO_2. A map of the site is shown in Fig. 1. Instruments to measure CO_2, CH_4, CO, N_2O and $\delta^{13}CO_2$ in near-surface air and X_{CO_2} in the column were located 3 km due north of the NPS at the Northern site at a swimming pool, which was closed for the winter and ideally located on the southern edge of the town. To the east of the measurement site is the smaller town of Stirling North, while about 6 km to the west is Port Augusta airport where measurements of wind speed and direction were obtained from the weather station operated for the Australian Bureau of Meteorology. Another in-situ analyser was located at Miranda, about 23 km south of the NPS, in order to capture northerly CO_2 plumes from the NPS, and to provide background measurements under southerly wind conditions. The Port Augusta city edge and Miranda sites are referred to as the Northern and Southern measurements sites respectively in this paper.

2.2 Instrumentation

The campaign included both solar remote sensing and in situ measurements using Fourier Transform spectrometers (FTSs). Two separate instruments were based on small (30 cm cube, $\sim$ 14 kg), 0.5 and 1 cm^{-1} resolution FT spectrometers (IRcube, Bruker Optics, Ettlingen, Germany) configured for either solar or in situ measurements.

2.2.1 Solar remote sensing

For solar remote sensing measurements, one IRcube was fitted with a CaF_2 beamsplitter and InGaAs detector and operated in the near infrared (NIR), 4000–10 000 cm^{-1} (1.0–

2.5 µm) covering CO_2 bands near 1.6 µm and O_2 near 1.27 µm. The solar beam was collected with an external heliostat which was actively aligned via a quadrant diode detector to keep the beam centred on the diode and FTS aperture. The parallel beam was fed into the IRcube via an off-axis parabola onto a 0.7 mm aperture. Data collection was automated from a single program under Windows which collected spectra and auxiliary analogue data (pressure, temperature, heliostat intensities) continuously. The measurement setup is in principle similar to that used by TCCON (Wunch et al., 2011b) but with reduced resolution.

On each measurement day the instrument was placed on a sturdy table, under cover from potential weather, and aligned to the solar beam from the heliostat. The intensities from the heliostat quadrant diodes were subsequently used as a quality control flag to remove spectra affected by clouds. The calculation of the final data product, the column-averaged dry air mole fraction X_{CO_2}, follows closely the method and procedures used by TCCON described in Wunch et al. (2011b) and is only summarised here. The 2009 version of the GGG software package developed for TCCON processing was used.

Spectra were first computed from the measured interferograms including correcting the raw interferograms for solar intensity variations (due to passing light cloud or other scattering effects) and phase errors as implemented in opus-ipp version 2.4.1. The computation of CO_2 and O_2 total column abundances (from the ~~average~~ combination of two CO_2 bands centred at 6228 and 6348 cm^{-1} and the 1.27 µm O_2 band centred at 7882 cm^{-1}) was achieved using the nonlinear least squares algorithm GFIT, version 4.4.2, which is described in appendix A(c) (i) of Wunch et al. (2011b). GFIT fits a computed solar atmospheric absorption spectrum at the measured solar zenith angle to each measured spectrum, and the trace gas amounts are retrieved from the fit. A departure from the standard TCCON processing was the use of European Center for Medium range Weather Forecasting (ECMWF) meteorology interpolated to the time of measurement for each spectrum. This ancillary meteorological data is used in the computation of the layer-by-layer absorption cross sections in GFIT. The standard TCCON meteorology is based on 6 hourly reanalysed NCEP fields interpolated to midday. This additional analysis step was introduced to test whether the spectra from low resolution spectrometers might be more susceptible to airmass depen-

dence at low zenith angles (i.e early morning and late afternoon) than high resolution data from TCCON HR125 spectrometers.

The CO_2 total column abundances were converted to X_{CO_2} by dividing by the total column of dry air, which is derived from the O_2 band in the same spectra. X_{CO_2} is corrected for the known airmass dependent artefact, a 1 % effect from spectroscopic induced errors, and the TCCON in-situ correction factor of 0.989 determined from careful comparison with a number of in-situ profiles as described by Wunch et al. (2010).

2.2.2 In situ measurements

In situ measurements were made using two FTIR trace gas analysers built at the University of Wollongong, one at the Northern (city) site, one at the Southern site. The analysers are described in detail by Griffith et al. (2012) and are equivalent to the now commercially available Spectronus analyser (Ecotech, Knoxfield, Australia). In summary, dried sampled air was collected from a mast 10 m above ground through Dekabon tubing and passed at 1 L min^{-1} and 1100 hPa through a 3.5 L sample cell with 24 m multipass optical path. The mid IR transmission spectrum of the sample was recorded continuously by the IRcube FTIR spectrometer with 1 cm^{-1} resolution, and the measured spectra fitted by non linear least squares to retrieve the trace gas composition of the sampled air. By analysing several spectral regions, the analyser provides simultaneous measurements of CO_2, CH_4, CO, NO_2 and $\delta^{13}CO_2$ with high precision and accuracy. For full details of the analyser, see Griffith et al. (2012).

In this application, spectra were averaged every 3 min (single scans take 1 s) to provide continuous 3 min data. The spectrometer was calibrated at the UoW laboratory against a suite of four reference gases supplied by CSIRO-GASLAB with mole fractions traceable to standard WMO reference scales. A single target tank, with known mole fractions of all species assigned from measurement against the four reference gases, was measured daily to detect any small drift in the spectrometer response. After correction with smoothed daily target tank measurements, all mole fractions are precise and accurate on WMO scales to better than 0.1 %.

3 Forward atmospheric transport model

For a finite domain, concentrations are influenced by sources within the domain, concentrations at the boundary and the initial condition. Assuming linearity of the transport operator (true in principle but usually not in practice), we can write the concentration at any point and time as

$$
\begin{aligned}
q(\boldsymbol{x},t) = &\int\limits_{\boldsymbol{\xi},\tau} T_s(\boldsymbol{\xi},\boldsymbol{x},\tau,t)s(\boldsymbol{\xi},\tau) \\
&+ \int\limits_{\boldsymbol{\xi}\in\mathcal{B},\tau} T_q(\boldsymbol{\xi},\boldsymbol{x},\tau,t)q(\boldsymbol{\xi},\tau) \\
&+ \int\limits_{\boldsymbol{\xi}} T_q(\boldsymbol{\xi},\boldsymbol{x},0,t)q(\boldsymbol{\xi},0),
\end{aligned}
\tag{1}
$$

where $T_s(\boldsymbol{\xi},\boldsymbol{x},\tau,t)$ denotes the transport of a source s from point $\boldsymbol{\xi}$ and time τ to point $\boldsymbol{x}$ and time t, $T_q(\boldsymbol{\xi},\tau,\boldsymbol{x},t)$ the transport of a concentration q from point $\boldsymbol{\xi}$ and time τ to point $\boldsymbol{x}$ and time t and $\mathcal{B}$ represents the boundary of the domain. Provided $t \gg 0$ we can replace the third term by a constant q_0, since any structure in the initial condition will have been transported out of the domain. We absorb q_0 into a constant needed to account for bias in the measurements noted in Sect. 2.2.

We use the on-line chemistry transport model WRF-CHEM (e.g. Grell et al., 2005) to model the other two terms in the equation.

3.1 WRF-Chem configuration

WRF is a regional-scale atmospheric transport model that is used for atmospheric research as well as operational forecasting (e.g. Givati et al., 2012). For the purposes of this study, we have used the chemistry version (WRF-Chem) of the Advanced Research WRF (ARW) dynamic core version 3.4.1 (e.g. Skamarock and Klemp, 2008). The model, which has a

~~non-hydrostatic~~hydrostatic pressure, terrain-following vertical eta-coordinate system, computes meteorological and tracer fields and it conserves mass, momentum and entropy. In this study, the Lambert conformal projection ~~is used as the model horizontal coordinates~~has been used to map real data to the surface of the Earth. In the vertical, the model has 30 levels with increased vertical resolution in the first few levels in the boundary layer (first few levels are at 10,25,52,98,197,297,496,762,1015m AGL) with the top of the model extending up to 50 hPa (altitude of about 20 km for the latitudes in South Australia). We have used three nested domains centred near the measurement site and the NPS in Port Augusta (32.5° S, 137.75° E). Domain resolutions are 9, 3 and 1 km. We allow feedback between the model domains. A map of the domains is shown in Fig. 2.

WRF-Chem can be run with a wide choice of physical and dynamical schemes. We use the Goddard and the Rapid Radiative Transfer schemes for the long-wave and short-wave radiation~~respectively~~, respectively, with a radiation time-step of 9 min, and the NOAH land surface model (Chen and Dudhia, 2001). A summary of physics schemes used in the model runs is presented in Table 1.

For the results presented in this study, we have used the WRF-Chem v3.4.1 with the WRF-GHG option switched on so that the model has been used as a tracer with no chemistry. The WRF-GHG option considers tracer advection of greenhouse gases in which WRF-Chem is coupled to the diagnostic biosphere model, the Vegetation Photosynthesis and Respiration Model (VPRM) (Mahadevan et al., 2008) In the coupled WRF-VPRM model, the Gross Ecosystem Exchange (GEE) is calculated using MODIS-derived land surface water index (LSWI), enhanced vegetation index (EVI), and shortwave radiation as well as WRF-derived surface temperatures. Respiration fluxes are simply derived as linear functions of the simulated temperatures (Ahmadov et al., 2007, 2009).

3.2 Initial and lateral boundary conditions

WRF-Chem needs initial and boundary conditions for dynamical variables and tracer concentration. Driving meteorological fields were taken from regional analyses by the Australian Bureau of Meteorology's Australian Community Climate and Earth-System Simu-

lator (ACCESS-A) model (now known as ACCESS-R) available at a resolution of $0.11°$ (about 12 km) and sampled every 6 h. For CO_2 initial and boundary conditions, we have used CO_2 forecasts from the Monitoring Atmospheric Composition and Climate (MACC-II) program (Agustí-Panareda et al., 2014) (https://www.gmes-atmosphere.eu/news/co2_forecasts/). These MACC CO_2 forecasts are obtained from ECMWF's Integrated Forecast System (IFS), where the CO_2 forecasts are run every day but initialised two days behind real-time in order to utilise near-real-time biomass burning emissions as estimated from satellite observations.

3.3 Potential sources of CO_2 emissions in Port Augusta

The dominant source of CO_2 at Port Augusta is the NPS, a 544 MW coal-fired power station that supplies electricity to South Australia. The NPS has annual carbon emissions in excess of 0.5 Tg C. Other anthropogenic sources of CO_2 include the towns of Port Augusta and Stirling North, the steel-works at Whyalla 60 km to the south-west of Port Augusta and the coal mine at Leigh Creek 250 km to the north that supplies the NPS. Whyalla steel-works is estimated to generate 0.63 Tg C annually, with 95 % being generated from direct steel making alone and the rest from indirect power generation (http://onesteel.sustainability-report.com.au/environment-2). Of these sources, only the town emissions are expected to contribute significantly at the measurement site due to their proximity. Emissions from Whyalla will contribute only under unfavourable wind conditions, while the emissions from Leigh Creek are expected to be tiny in comparison with those from the NPS.

Natural sources of CO_2 within the region surrounding Port Augusta include the biosphere through plant photosynthesis and fire. Indeed, there were uncontrolled bush fires to the east in the Flinders Ranges especially during the last few days of the measurement campaign. These days have been excluded from the analysis of results presented in this paper.

Modelling the in-situ and column CO_2 concentrations must account for these sources in order to attribute the measured CO_2 signals accurately. ~~We have assigned these emissions (except from bush fires)~~ With the exception of bushfires, we have assigned point source

10

emissions from the NPS, area source emissions from Port Augusta town and the biosphere in the model as different tracers in order to account for their relative contributions to the observed signal in Port Augusta. We have neglected emissions from Whyalla Steelworks, Leigh Creek and Stirling North for the reasons suggested above. For the NPS CO_2 fluxes, we have used National Electricity Market-wide Carbon Dioxide Equivalent Intensities by using real-time live energy output from the NPS as published by the Australian Energy Market Operator (AEMO) (http://www.aemo.com.au/About-AEMO). The ~~NPS~~ emissions from the power plant are calculated as the product of recorded despatch power of the power plant and the Carbon Dioxide Equivalent Intensity index (0.948 in the case of the NPS). The NPS emissions are input into the model at level 6 representing stack height at 200m above ground. The other tracers are emitted at the first model level (about 10m above ground) The NPS fluxes are not constant but vary with energy demand. Data on energy output is available with five minute temporal resolution. For input in the model, the fluxes are averaged per hour.

4 Measured data

Concentrations of CO_2~~and~~, CH_4, CO, N_2O and $\delta^{13}CO_2$ in near-surface air and ~~column-averaged~~ X_{CO_2} were measured during the Port Augusta measurement campaign. In this paper, we use concentrations of CO_2 and CO in near-surface air and column-averaged X_{CO_2} in order to disaggregate the influence of local and regional sources. The in-situ measurements are influenced to a greater extent by sources and sinks in the immediate environment as well as the evolution of the boundary layer. On the other hand, X_{CO_2} is an average along the path from the measurement site to the sun, so it is less sensitive to local sources and sinks and changes in boundary layer height, and generally has lower spatial and temporal variability.

4.1 Measured in-situ data

Wind speed and direction for the duration of the campaign, shown in Fig. 3, were derived from the weather station maintained by the Bureau of Meteorology at Port Augusta airport, about 6 km to the west of the measurement site. From 7 to 9 May 2012, the wind was generally from the north and north-west with speed varying from 4–10 m s^{-1}. After 9 May the synoptic pattern changed, and the wind was mainly from the south and south-east with speed ranging from 2–10 m s^{-1}.

Figure 3a and b is the time series of in-situ concentrations of CO_2 and CO measured at the Northern site in Port Augusta. The diurnal variations in the concentrations are functions of both the planetary boundary layer (PBL) heights and the local meteorology through dilution and advection of their respective fluxes. For these reasons, CO and CO_2 are largely correlated (correlation coefficient of 0.65).

The differences between them can be attributed to their different sources since the nearby NPS is a major source of CO_2 whereas CO is mainly a marker for the town source. During the early phase of the data (between 7 and 9 May) with north and north-north-west winds, we do not see much structure in either the measured in-situ CO_2 or CO. The winds are blowing over the town towards the NPS, so we do not expect to see the NPS CO_2 plume in the data. However, during this time, we do not seem to see much of the CO either. The observed low CO_2 and CO levels are perhaps a consequence of dilution due to the high wind speeds during the day. After 9 May, the variable wind direction and speeds allows the plume from the NPS to be advected towards the measurement site so that during this period there is increased structure in measured CO_2 and CO concentrations. Most of the measured peaks are however occurring at night, following the collapse of the PBL. There are times when we see peaks in measured in-situ CO_2 but not in CO and vice-versa. For example, on 14 May at noon, we see a peak in surface CO_2 of 405 ppm but no corresponding peak in CO. On this occasion, we have southerly winds and relatively higher wind speeds (8 m s^{-1}) blowing CO_2 from the NPS towards the measurement site. This is also repeated, although to a lesser extent, on 13 May and 15 May at around midday.

12

Time series of in-situ CO_2 concentrations measured at the Northern site 3 km north of the NPS have been plotted alongside those measured at the Southern site 22 km south of the NPS as shown in Fig. 4a. Clearly, there are several peaks or high concentration CO_2 episodes that were observed at the Northern site but not at the Southern site. These can only be attributed to the NPS. We do not expect to see much of the NPS plume at the Southern site as it is ~~too~~ so far from the NPS ~~for the plume to touch down~~that the plume is diluted by the time it arrives at the Southern site. The elevated concentrations measured at the Southern site on 10 May are probably due to bush fires burning in the Flinders Ranges to the east of the Southern site, as confirmed by elevated CO concentrations measured at the Southern site (Fig. 5). Overall a comparison of CO measured at the two sites (Fig. 5) shows more structure at the Northern site than at the Southern site. This is expected given the proximity of the Northern site to local CO sources in the surrounding towns of Port Augusta and Stirling North, both of which are much larger than Miranda town at the Southern site.

4.2 Measured column-averaged data

Unlike in-situ data which samples the local or immediate environment, column-averaged data samples the whole column of air so it is relatively immune from being dominated by local sources. In Fig. 3c, we see time series of X_{CO_2} measured at the Northern site plotted alongside the in-situ data (Fig. 3a and b) to aid comparison. The signal strengths for the in-situ CO_2 measurements (from 387 to 415 ppm) are larger than those for the X_{CO_2} measurements (391 to 394 ppm) by a factor up to 10. Unlike the in-situ data, the larger volume of air sampled in the column-averaged data means that much of the sampled concentration in the column is unaffected by both local sources and dilution and concentration caused by the diurnal expansion and contraction of the PBL height. The in-situ CO_2 time series generally peak at night due to the collapsed PBL height, and decrease with the onset of day caused by dilution as the PBL height deepens. It is also clear from Fig. 3 that the differences in the variations in the signals between in-situ and column-averaged are not only caused by boundary layer effects, but also the fact that the two instruments are sampling air masses at disparate spatial scales. For example, peaks in X_{CO_2} do not always coincide with peaks

in in-situ CO_2 concentrations (e.g. on 11 May). Nevertheless, occasionally we see daytime peaks (such as on 9 and 14 May) in the in-situ CO_2 data coinciding with peaks in the X_{CO_2} data. This ~~suggests~~ may likely be attributed to plume touch down at the Northern site.

5 Modelled data

Using WRF-Chem coupled to a biospheric model (as described in Sect. 3.1), we have simulated in-situ CO_2 and X_{CO_2} concentrations at the Northern Site and compared them with observed data. The model results presented here are from the highest spatial resolution (1 km) domain in order to resolve the CO_2 fields between the Northern site and the NPS 3 km to the south. The temporal resolution in model output was every five minutes, although in the comparisons we averaged both the model output and the observations over half-hourly intervals.

Whereas the modelled in-situ data is simply taken from the model grid cell at the location in which the measurements were made, analysis of the column data is more complex. X_{CO_2} concentrations in the model domain have been computed along a slant path (rather than vertical) to the top of the model by calculating the path through each grid cell as a function of sun position. As the model top is only at 50 hPa, there is need to account for the extra contribution, denoted δX_{CO_2}, from CO_2 between the model top and space. For this work, we assumed that δX_{CO_2} is related to the true X_{CO_2} via

$$\delta X_{CO_2} = \left(\frac{p_{\text{model top}}}{p_{\text{model bottom}} - p_{\text{model top}}} \right) X_{CO_2}, \tag{2}$$

and added δX_{CO_2} to the column-average computed from the model. In order to compare the total simulated X_{CO_2} with the observed X_{CO_2}, we have accounted for the instrument-dependent averaging kernel and prior profile used in the X_{CO_2} retrieval following the work of Connor et al. (2008).

14

5.1 Modelled vs. observed meteorology

How well the transport model simulates the observed in-situ and column-averaged CO_2 concentrations depends to a large extent on how well it predicts the meteorology (wind speed and direction). We compare the simulated wind data with observations made at Port Augusta airport, about 6 km west of the Northern site. As shown in Fig. 6, the model's simulation of wind direction is broadly similar to observed data, with northerlies during the early phase of the campaign and variable wind direction for the rest of the measurement period, although it seems there is much more variability in the modelled wind direction than there is in the observations. Nevertheless, on 11, 12 and 14 May, the modelled wind direction is in good agreement with observations. Similarly, for simulated and observed wind speed at Port Augusta airport (Fig. 7), the diurnal profiles are broadly in agreement, although we see higher observed daytime wind speeds than in the model by as much as 3 or 4 m s^{-1}, perhaps caused by the sea breeze. The differences in modelled and observed wind speeds may lead to mismatches in the timing of observed and simulated mixing ratios.

5.2 Modelled vs. measured CO_2

5.2.1 In-situ CO_2 concentration

We present a detailed comparison of modelled and measured CO_2 mole fractions. The limited number of sources means we can use the Pearson correlation coefficient as a measure of the similarity of two time-series. It is particularly convenient since it is independent of the source magnitude.

Since predicted signals in the model domain are due to both local emissions as well as upwind boundary signals entering the model domain, it is important to include the boundary conditions in the model simulation. Thus all the tracers (NPS tracer, town tracer, biospheric tracer, etc) have been simulated with initial and boundary conditions included from regional MACC CO_2 fields. These fields, which are obtained at a resolution of 50 km × 50 km, have been interpolated onto the model outer domain. As the NPS is not included in the back-

ground, deviations from the simulated background concentrations should be due to the local emissions. Another reason for including the background in the simulated tracers is practical, serving as a positive offset, thus avoiding negative concentrations that have been known to be associated with sharp gradients, even with positive definite advection schemes (Beck et al., 2011).

Figure ?? 8 shows the time series of measured and simulated night-time and daytime in-situ concentrations of CO_2 with tracers from the town and the NPS shown separately. Surface concentrations are particularly subject to diurnal variation effects of the PBL, so most of the peaks in the observed and simulated concentrations occur at night when the PBL height has collapsed. Strong atmospheric inversions at night suppress mixing of surface air with air from above, thus isolating the NPS plume from the measurement site. The variation in the town tracer does not show much structure, except for a typical diurnal profile due to the PBL. On the other hand, for the NPS tracer, there is much more structure with some peaks occurring during the day and these tend to agree with observations. However, there seems to be a time-delay in the simulated NPS tracer so that simulated peaks on 9, 11 and 12 May occur about 1, 6 and 3 h after the observed peaks, respectively. The largest peak in simulated surface CO_2 (418 ppm) on 10 May is not reproduced by the observations. This, plus the delayed peaks, generates a correlation between observed and simulated in-situ CO_2 concentrations of -0.05. The delayed simulated CO_2 peak concentration can be attributed to the lower simulated wind speeds relative to observations. This is most likely caused by the model's poor simulation of sea breeze. With difference in wind speeds of about $3 \, \mathrm{m \, s^{-1}}$, and for a distance of 3 km, delays of about 2 h are conceivable but not delays of 6 h, which may be caused by recirculation of air masses over a longer distance. It is therefore tempting to match the peaks in simulated concentrations in order to account for the sea breeze error as shown in Fig. ?? 9. This improves the correlation somewhat to 0.42 . which is still poor. This underscores the deficiencies of the model to simulate the in-situ tracer under the given synoptic conditions.

16

5.2.2 Column-averaged CO₂ concentration

Since the X_{CO_2} measurements are made only during daytime with a sun-staring instrument, for comparison with simulated data it is helpful to plot individual days separately. Measured and simulated <u>(from the NPS tracer)</u> time series of half-hourly averaged X_{CO_2} are plotted for 8, 10, 11 and 14 May 2012 as shown in Fig. 10a–d respectively. The data have been averaged in order to remove noise that cannot be resolved by the model. For these plots, the simulated data contains both the NPS source as well as background concentrations from MACC CO₂. The first thing to note about the observed and simulated X_{CO_2} is the difference in magnitude of up to 0.6 ppm. This ~~is unimportant as the~~ <u>does not affect the emissions estimates, because the</u> mean level is ~~calculated explicitly~~ <u>explicitly calculated</u> by the inversion~~so does not affect emissions estimates~~. However, the structure in the observed and simulated time series are broadly similar, which is encouraging. Secondly, the signal enhancements in measured and simulated X_{CO_2} are much weaker than for in-situ data, with maximum signal enhancement of about 2–3 ppm compared to 15–20 ppm. The ratio is similar to that of the boundary layer thickness to the atmospheric column mass. The power-plant tracer explains much more of the variation in measured X_{CO_2} than it does for the in-situ dataset. Indeed, comparison between observed and simulated X_{CO_2} and in-situ CO₂ gives correlation coefficients of 0.72 and 0.42 respectively, although for the in-situ case time-shifting is employed in order to match the peaks. A plot of measured vs. simulated X_{CO_2} is shown in Fig. 11.

The lateral boundaries play a much larger role in simulated X_{CO_2} than they do for in-situ simulations. This was previously noted by Lauvaux et al. (2008) when comparing airborne and surface measurements.

The importance of the background is demonstrated in Fig. 12, which shows that variations of up to 1 ppm are caused by regional-scale transport of MACC CO₂ from the boundary. Since the NPS source is not included in the background X_{CO_2}, deviations from background X_{CO_2} are due to the NPS source. For some of the days early in the time series (such as on 8 and 9 May) the magnitudes of the simulated background and NPS concentrations are

identical, which means that for those days the NPS tracer was not visible in the measured X_{CO_2}, consistent with the observed prevailing northerlies during the early phase of the measurement campaign.

6 Estimating emissions

One of the goals of this study is to understand the factors that control the accuracy with which CO_2 emissions from a point source such as the NPS may be estimated using in-situ and column-averaged CO_2 concentrations. Assuming linearity of the transport model, the CO_2 concentration observed at the measurement site is the sum of the background concentration and concentrations from local emissions.

Thus, subtracting the simulated background concentration from both the observed and simulated tracer concentrations should give the CO_2 fingerprint due to the NPS alone. Using this fingerprint, we calculate a multiplier for the emission rate (which also can be chosen arbitrarily) used in the model run. The simplicity of the system (one isolated source) means we can avoid the complexities of the normal Bayesian setup (e.g. Ciais et al., 2010) and calculate this multiplier using simple linear regression. For the model results presented in this paper, we have used the actual CO_2 emissions from the NPS, which have been obtained from the National Electricity Market-wide Carbon Dioxide Equivalent Intensities as published by AEMO. Thus we expect an emission multiplier of unity.

In Table 2 are shown the calculated emission factors, uncertainties, root-mean-square error (RMSE) of the model-data mismatches and the correlation coefficients between measured and simulated (source + background) and measured vs. simulated (source only) using in-situ and column-averaged CO_2 data. Even with time-shifting (in order to account for sea-breeze) to match the peaks in the simulated and measured in-situ data, the linear regression still yields a poor multiplier of 0.12, and poor correlation coefficients (0.30 with source + background and 0.4 with source only). However, the story is different with column-averaged data, which gives a better correlation (0.72 for source + background and 0.67 for source only). An emission factor of 1.06 is within 6 % of the target value, although the un-

certainty of ± 0.54 is larger than for surface data, due both to fewer data and small signals of the NPS in the column-averaged data. Using the column-averaged data gives smaller model-data mismatches with RMSE of 0.44 ppm, which is almost half that of in-situ data (0.78 ppm).

7 Discussion

Recently, Lindenmaier et al. (2014) conducted simultaneous in-situ and column measurements of CO_2, CO, NO_2 and $\delta^{13}CO_2$ in the vicinity of ~~four~~ two large power plants (the Four Corners Generating Station and the San Juan power plant) with different scrubbing technologies at the Four Corners Generating station near Fruitland, New Mexico, USA. In their study, they found strong correlations between column and in-situ observations of CO_2, SO_2, CO and NO_2 measured during plume events. They also found distinct $\Delta NO_2/\Delta CO_2$ ratios in the polluted air masses (dependent on power plant scrubbing technologies), and they postulated that, by conducting long-term measurements of column $\Delta NO_2/\Delta CO_2$ concentrations near point sources, the trends can be used for emission verification purposes ensuring adherence to and improvement in scrubbing technologies. By comparing regional column $\Delta NO_2/\Delta CO_2$ and in-situ measurements they concluded that 70–75 % of the stable regional atmosphere in the vicinity of the power plants was polluted, which underscores the influence of power plant sources. This result is in agreement with our sampling of the air mass in the vicinity of the power plant in Port Augusta.

We have found evidence for increased in-situ and column-averaged CO_2 concentrations in the vicinity of the NPS. However, increases in in-situ concentrations do not always correlate with column concentrations because of local contamination from the town or because the plume does not touch down at the Northern site. The agreement is better during the few days of favourable meteorological conditions when southerlies carry the NPS CO_2 plume to touch down at the measuring site. The timing in the peaks does not always match the simulation probably due to poor simulation of the sea breeze. Although it is one of the most theoretically studied weather phenomenon current generation numerical

weather prediction (NWP) models still struggle to accurately predict the onset and extent of sea breeze (e.g. Chen et al., 2011). We note that wind speeds simulated at Port Augusta airport about 6 km west of the measurement site are mostly slower than observed winds speeds by up to 4 m s^{-1}. Matching of the in-situ peaks in order to account for sea breeze requires time-shifting by 1 to 6 h. Whereas 1 to 2 h delay can be envisaged from such wind speed differences for a distance of 3 km, time-shifting by 6 h is unlikely caused by this, and may be explained by either recirculation or simply deficiencies in the model. The picture is, however, different for column-averaged concentrations, which are more immune to ~~local contamination as~~ locals sources (such as traffic) in the immediate vicinity as they are averaged over a larger body of air than localised in-situ concentrations. Thus, it is expected that the model should simulate column-averaged concentrations better, giving better correlations between the simulated and observed data.

The importance of the background concentrations in regionally averaged air masses is shown from the simulated MACC CO_2 concentrations with enhancements of up to 1 ppm in the simulated column concentrations. Subtracting the background from the total simulated CO_2 concentration enables us to resolve the influence of local sources on the net simulated CO_2 concentration. Assuming one major isolated source, inversion synthesis through simple linear regression of variations in the observed and simulated concentrations enables independent calculation of the fluxes from the source, which can be compared with published emissions data. From our study, we calculate emissions from the NPS that are within 6 % of the published data. ~~To our knowledge, this is the first time such a calculation has been attempted. It is therefore~~ It is instructive to assess the sensitivity of our emission calculation to model parameters such as model resolution, model type (i.e. whether Eulerian or Lagrangian), input emission profile and injection height, and model output data frequency among other factors.

7.1 Model spatial resolution

For domain resolution, our choice of 1 km resolution in the innermost domain (high end on the resolution scale for mesoscale models) has been necessitated by the require-

ment to resolve the short 3 km distance between the power plant and the measurement site. We can increase the resolution of the model but this will push our model towards turbulence-resolving large-eddy simulation (LES) mode. Such high resolution models offer the advantage of resolving small-scale spatial dynamics, especially over complex terrain. However, apart from the increased computing expense, increased model resolution does not necessarily lead to improved simulation of regionally averaged simulation outputs, as was observed by Talbot et al. (2012) where they found that the most important control on mesoscale model results was not resolution but the quality of the meteorological forcings that drive the model.

7.2 Model choice: Lagrangian or Eulerian

On the other hand, a deficiency of 3-D Eulerian models in simulating plumes is their inherent assumption that the concentration field is uniform across the whole grid-cell. This assumption breaks down in the case of narrow plumes, such that one is forced either to increase model resolution or to use alternative Lagrangian models that are more amenable to advection of narrow plumes. However, whereas Lagrangian models are ideally suited to simulation of in-situ data, Eulerian models are better for the simulation of column-averaged data (because of their clearly defined vertical structure in the 3-D grid cells).

Faced with which model to use, during the early part of our study we experimented with using the Lagrangian model CALPUFF, which is a multi-layer, non-steady state puff dispersion model (e.g. Levy et al., 2002). However, the results (not presented here) were inferior to those obtained from WRF-Chem. Using a model resolution of 1 km, it was found that CALPUFF needed extensive spatial and vertical tolerance to simulate reasonably both in-situ and column-averaged data. Although the reasons for its poor performance are not obvious, it was thought that the model struggled because of sea breeze effects.

7.3 Emission injection height and plume rise

For the results presented above, the emissions in the model, which assume no plume rise, have been injected into the model level that corresponds to the stack height of 200 m for the NPS (model level 6). We have assessed the sensitivity of the model results to changes in emission injection height, and also experimented with explicit plume injection height calculations. For the town tracer, CO_2 emissions have been assigned in the bottom level of the model, which is about ~~50~~10 m high. However, for the NPS tracer, its emissions are assigned according to four scenarios where emissions are released at model levels 5, 6 and 7 (denoted L5, L6 and L7) and also at multiple levels from the stack height using plume rise calculations (hereafter PR). The plume rise calculations used are based on algorithms from the Regional Acid Deposition Model (RADM) (Byun and Binowski, 1991) following the work of Briggs (e.g. Briggs, 1969, 1984). The algorithm considers layer-by-layer plume penetration due to either momentum lift or buoyancy (whichever is greater) by considering three stability regimes (neutral, stable and unstable). We present model results from the simulated concentrations from each of these emission scenarios.

Two separate passive CO_2 tracers, one from the NPS and another from the towns of Port Augusta and Stirling North, are tracked in the model. As shown in Table 3, changing emission injection height does not greatly affect the model result, with the emission multipliers tending towards unity (i.e. the truth) as model emission injection height is increased, giving multipliers of 1.06, 1.05, 1.0 and 1.0 for emission injection heights L5, L6, L7 and PR, respectively. There is negligible change in uncertainty values with L5 and L6, giving identical values of ± 0.54, and ± 0.55 for L7 and PR. The RMSE are also largely unchanged, ranging from 0.44, 0.44, 0.46 and 0.45 ppm for L5, L6, L7 and PR respectively. Simulated column-averaged CO_2 gives best correlation with observation with correlation coefficients of 0.72 (with background) and 0.67/0.68 (without background) for L5 and L6 respectively. Correlation coefficients from L7 and PR runs are poorer (0.68 and 0.69 with background and 0.63 and 0.64 without background). The result is thus insensitive to model emission

injection height. Implementation of a plume rise calculation in the emission profile improves the multiplication factor, although the uncertainty is slightly increased.

7.4 Other sources of CO_2

As was explained in Sect. 3.3, apart from the NPS as a major source of CO_2 in the immediate vicinity of the measurement site, other sources include the town, emissions from Whyalla steel-works 60 km to the south-west and the biospheric source. Although the Whyalla steel-works is a large CO_2 emitter, from our correlation of the Whyalla tracer with in-situ and column-averaged CO_2 observations (not shown here), we have found no evidence of Whyalla CO_2 tracer at the Northern site. This is either because most of the air masses originating from the southern edge of the domain do not reach the Northern site and/or, if it does, by the time the air mass has travelled 60 km to reach the measuring site, its strong source of CO_2 is already mixed well (and hence diluted) to background concentration. The same can be said of CO_2 from the city of Adelaide about 290 km south.

The biosphere is a major source and sink of CO_2 through plant photosynthesis and respiration. The region around NPS is not very productive but the Flinders Ranges to the east are more biospherically active and thus expected to contribute to the observed CO_2 concentration at the Northern site. With the WRF-GHG option switched on, the model is coupled to the VPRM model (Ahmadov et al., 2007, 2009), as explained in Sect. 3.1. A map of net biospheric fluxes, which have been generated using the VPRM preprocessor, are plotted in Fig. 13. The eastern side of the domain is dominated by net sources of up to $12\,000\,\mathrm{mol\,km^{-2}\,h^{-1}}$ of CO_2 (about $528\,\mathrm{kg}$ of $CO_2\,\mathrm{km^{-2}\,h^{-1}}$), although there are some areas which are net sinks of up to $-25\,000\,\mathrm{mol\,km^{-2}\,h^{-1}}$ (about $-1100\,\mathrm{kg}$ of $CO_2\,\mathrm{km^{-2}\,h^{-1}}$). The biospheric net source of $12\,000\,\mathrm{mol\,CO_2\,km^{-2}\,h^{-1}}$ (equivalent to a typical flux of $4625\,\mathrm{t\,CO_2\,km^{-2}\,year^{-1}}$) is tiny compared to the fluxes from the NPS (which are a factor of about 800 times greater, for a given average flux rate of $427\,\mathrm{t\,CO_2\,km^{-2}\,h^{-1}}$), again showing that the NPS is the major source of CO_2 in the area. Figure 14 shows timeseries of simulated column-averaged CO_2 concentrations for the NPS tracer, background tracer and the biospheric tracer. The net biospheric fluxes contribute to enhancements in

23

the column of 0.39 ppm maximum (average of 0.16 ppm) above the background tracer, compared to 1.1 ppm maximum enhancement above background (average of 0.37 ppm) for the NPS tracer. Compared with observations, the biospheric column CO_2 gives correlation coefficients of 0.54 (with background) and 0.59 (without background).

7.5 Limit on time resolution of data

For the foregoing results, the model data was sampled every five minutes from which were calculated half-hour averages to compare with similarly averaged observation data. This choice is driven by experience of the trade-off between using more data (hence lower uncertainty) and the limits of model skill. An important question is what frequency of variation is predictable and how much is noise from both the instrument and the model simulation? The answer to this question depends not only on the prevailing meteorological conditions but also on the model resolution and instrument precision. It is expected that the model cannot resolve sampled data within a few minutes of each other, so that five minutely sampled data should not be too different from data sampled every ten minutes unless the model tracer field is changing very rapidly As shown in Table 4, changing the model data sampling time from 5, 10 and to 20 min changes the calculated emission factor from 1.05 ± 0.54, 0.99 ± 0.56 and 0.80 ± 0.61 respectively. Thus all changes are within the $1 - \sigma$ uncertainty of all estimates. The increased uncertainty is due to the reduced sample size which is itself caused by gaps in measured data.

7.6 Case with unknown emission time profile

The results presented above have been calculated by using data from a power plant with known emission time (the diurnal) profile as provided from the Australian Energy Market Operator (AEMO). What are the implications for sources where no such detailed time profiles are available? To test the sensitivity to this, we have run the model with constant emissions.

As shown in Table 5 using a constant CO_2 flux of $401.4 \, \mathrm{t \, km^{-2} \, h^{-1}}$, we get (surprisingly) better correlations of 0.78 and 0.72 (source plus background and source only, respectively)

compared to the AEMO emission case which gives 0.72 and 0.67 (source plus background and source only, respectively). The constant emission run also gives slightly better RMSE of 0.41 (vs. 0.44 for the diurnal emission case) but has a slightly worse uncertainty (0.60 compared to 0.54 for the diurnal emission run). The emission factor of 1.32 ± 0.60 from the constant emission run is a factor of 1.25 greater than that obtained using prescribed diurnal profile. ~~This underscores the importance of using an accurate description of the given emission profiles and shows the risks of using a fixed emission profile in a situation where in reality, the emissions have diurnal profile~~However, this emission factor is still within the interval of the original estimate, which points to deficiencies in the modelling and/or lack of sufficient data.

8 Conclusions

We have developed portable instruments for measuring column-integrated CO_2 with reasonable accuracy. These instruments can detect signals from a moderate sized power-plant at a distance of 3 km although the signals are much weaker than those from surface in situ mesurements at the same location. High-resolution mesoscale simulations compare much better with the column-integrated measurements than with the in situ. Using column-integrated measurements in a simple inverse model we can estimate the power-plant emissions with an error of ~~5~~6 % using 6 days of measurements. ~~The~~ However, the small size of the dataset used in this study has led to large uncertainties. Future work will address these uncertainties by collecting measurement data over a longer period. Nevertheless, the preliminary results suggest that column-integrated measurements offer a good compromise between sensitivity and the capability of current mesoscale models for estimating emissions from point sources.

was undertaken on the NCI National Facility in Canberra, Australia, which is supported by the Australian Commonwealth Government.

References

Abshire, J. B., Ramanathan, A., Riris, H., Mao, J., Allan, G. R., Hasselbrack, W. E., Weaver, C. J., and Browell, E. V.: Airborne measurements of CO_2 column concentration and range using a pulsed direct-detection IPDA lidar, Remote Sens., 6, 443–469, ~~2014.~~ 2013.

Agustí-Panareda, A., Massart, S., Chevallier, F., Boussetta, S., Balsamo, G., Beljaars, A., Ciais, P., Deutscher, N. M., Engelen, R., Jones, L., Kivi, R., Paris, J.-D., Peuch, V.-H., Sherlock, V., Vermeulen, A. T., Wennberg, P. O., and Wunch, D.: Forecasting global atmospheric CO_2, Atmos. Chem. Phys., 14, 11959–11983, doi:10.5194/acp-14-11959-2014, 2014.

Ahmadov, R., Gerbig, C., Kretschmer, R., Koerner, S., Neininger, B., Dolman, A. J., and Sarrat, C.: Mesoscale covariance of transport and CO_2 fluxes: evidence from observation and simulations using the WRF-WPRM coupled atmosphere–biosphere model, J. Geophys. Res., 112, D22107, doi:10.1029/2007JD008552, 2007.

Ahmadov, R., Gerbig, C., Kretschmer, R., Körner, S., Rödenbeck, C., Bousquet, P., and Ramonet, M.: Comparing high resolution WRF-VPRM simulations and two global CO_2 transport models with coastal towerthe peaks. A
measurements of CO_2, Biogeosciences, 6, 807–817, doi:10.5194/bg-6-807-2009, 2009.

Andres, R. J., Boden, T. A., Bréon, F.-M., Ciais, P., Davis, S., Erickson, D., Gregg, J. S., Jacobson, A., Marland, G., Miller, J., Oda, T., Olivier, J. G. J., Raupach, M. R., Rayner, P., and Treanton, K.: A synthesis of carbon dioxide emissions from fossil-fuel combustion, Biogeosciences, 9, 1845–1871, doi:10.5194/bg-9-1845-2012, 2012.

Asefi-Najafabady, S., Rayner, P. J., Gurney, K. R., McRobert, A., Song, Y., Coltin, K., Huang, J., Elvidge, C., and Baugh, K.: A multiyear, global gridded fossil fuel CO_2 emission data product: evaluation and analysis of results, J. Geophys. Res.-Atmos., 119, 10213–10231, doi:10.1002/jgrd.v119.17, 2014.

Australian Energy Market Operator (AEMO): 2013 South Australia Electricity Report, ABN 94 072 010 327, online report available at: http://www.aemo.com.au/Electricity/Planning/South-Australian-Advisory-Functions/~/media/Files/Other/planning/2013_SAER_Final_Report_Full.ashx, 2013.

Basu, S., Guerlet, S., Butz, A., Houweling, S., Hasekamp, O., Aben, I., Krummel, P., Steele, P., Langenfelds, R., Torn, M., Biraud, S., Stephens, B., Andrews, A., and Worthy, D.: Global CO_2 fluxes estimated from GOSAT retrievals of total column CO_2, Atmos. Chem. Phys. Discuss., 13, 4535–4600, doi:10.5194/acpd-13-4535-2013, 2013.

Beck, V., Koch, T., Kretschmer, R., Marshall, J., Ahmadov, R., Gerbig, C., Pillai, D., and Heimann, M.: The WRF Greenhouse Gas Model (WRF-GHG), available at: http://www.bgc-jena.mpg.de/bgc-systems/pmwiki2/uploads/Download/Wrf-ghg/WRF-GHG_Techn_Report.pdf (last access: 12 December 2014), 2011.

Briggs, G. A.: U.S. Army Environmental Center Critical Review Series TID-25075, USAEC Technical Information Center, Oak Ridge, TN, USA, 1969.

Briggs, G. A.: Plume rise and buoyancy effects, atmospheric sciences and power production, in: DOE/TIC-27601 (DE84005177), edited by: Randerson, D., TN. Technical Information Center, U.S. Dept. of Energy, Oak Ridge, USA, p. 850, 1984.

Byun, D. W. and Binowski, F. S.: Sensitivity of RADM to point source emissions processing, in: Paper 5.4 presented at the 7th Joint conference on Applications of Air Pollution Meteorology with the Air and Waste Management Association, New Orleans, 14–18 January 1991, LA. American Meteorological Soc, Boston, MA, USA, 70–73, 1991.

Chen, F. and Dudhia, J.: Coupling an advanced land surface hydrology model with the Penn State NCAR MM5 Modeling System. Part 1: Model implementation and sensitivity, Mon. Weather Rev., 129, 569–585, 2001.

Chen, F., Miao, S., Tewari, M., Bao, J. W.,and Kusaka, H.: A numerical study of interactions between surface forcing and sea breeze circulations and their effects on stagnation in the greater Houston area, J. Geophys. Res., 116, D12105, doi:10.1029/2010JD015533, 2011.

Chen, J., Gottlieb, E., and Wofsy, S.: Compact FTIR Spectrometer for total column measurement in urban environments, in: IRWG/TCCON Meeting, Wengen, Switzerland, 11–15 June 2012, avialable online at: http://people.seas.harvard.edu/~jiachen/images/Presentation_IRWG_Chen[CompatibilityMode].pdf 2012.

Chevallier, F., Deutscher, N. M., Conway, T. J., Ciais, P., Ciattaglia, L., Dohe, S., Frhlich, M., Gomez-Pelaez, A. J., Griffith, D. W. T., Hase, F., Haszpra, L., Krummel, P., Kyr, E., Labuschagne, C., Langenfelds, R., Machida, T., Maignan, F., Matsueda, H., Morino, I., Notholt, J., Ramonet, M., Sawa, Y., Schmidt, M., Sherlock, V., Steele, P., Strong, K., Sussmann, R., Wennberg, P. O., Wofsy, S. C., Worthy, D., Wunch, D., and Zimnoch, M.: Global CO_2 fluxes inferred

from surface air-sample measurements and from TCCON retrievals of the CO_2 total column, Geophys. Res. Lett., 38, 1–5, doi:, 2011.

Chou, M. D. and Suarez, M. J.: An efficient thermal infrared radiation parameterization for use in general circulation models, NASA Tech. Memo. 104606, 3, 85 pp., Climate and Radiation Branch, Laboratory for Atmospheres, NASA/Goddard Space Flight Center, Greenbelt, MD, 20771, 1994.

Ciais, P. I., Rayner, P., Logan, M. L., Peylin, P., Ramonet, M., Bousquet, P., Chevallier, F.: Combining top-down and bottom-up information for estimating CO_2 fluxes: methods and perspectives, Clim. Change, 103, 69–92, doi:10.1007/s10584-010-9909-3, 2010.

Connor, B. J., Boesch, H., Toon, G., Sen, B., Miller, C., and Crisp, D.: Orbiting carbon observatory: inverse method and prospective error analysis, J. Geophys. Res.-Atmos., 113, 2156–2202, 2008.

Enting, I. G.: Inverse Problems in Atmospheric Constituent Transport, Cambridge University Press, Cambridge, UK, 392 pp., 2002.

Enting, I. G.: Inverse Problems in Atmospheric Constituent Transport, Cambridge Univ. Press, New York, 412 pp., 2005.

Gisi, M., Hase, F., Dohe, S., Blumenstock, T., Simon, A., and Keens, A.: XCO_2-measurements with a tabletop FTS using solar absorption spectroscopy, Atmos. Meas. Tech., 5, 2969–2980, doi:10.5194/amt-5-2969-2012, 2012.

Givati, A., Lynn, B., Liu, Y., and Rimmer, A.: Using the WRF Model in an Operational Streamflow Forecast System for the Jordan River, J. Appl. Meteorol. Clim., 51, 285–299, doi:10.1175/JAMC-D-11-082.1, 2012.

Göckede, M., Markkanen, T., Hasager, C. B., and Foken, T.: Update of a footprint-based approach for the characterisation of complex measurement sites, Bound.-Lay. Meteorol., 118, 635–655, 2006.

Grell, G. A. and Dévényi, D.: A generalized approach to parameterizing convection combining ensemble and data assimilation techniques, Geophys. Res. Lett., 29, 38-1–38-4 doi:10.1029/2002GL015311, 2002.

Grell, G. A., Peckham, S. E., Schmitz, R., McKeen, S. A., Frost, G., Skamarock, W. C., and Eder, B.: Fully coupled "online" chemistry within the WRF model, Atmos. Environ., 39, 6957–6975, 2005.

Griffith, D. W. T., Deutscher, N. M., Caldow, C., Kettlewell, G., Riggenbach, M., and Hammer, S.: A Fourier transform infrared trace gas and isotope analyser for atmospheric applications, Atmos. Meas. Tech., 5, 2481–2498, doi:10.5194/amt-5-2481-2012, 2012.

Hong, S. Y., Noh, Y., and Dudhia, J.: A new vertical diffusion package with an explicit treatment of entrainment processes, Mon. Weather Rev., 134, 2318–2341, 2006.

House, J. I., Prentice, I. C., Ramankutty, N., Houghton, R. A., and Heimann, M.: Reducing apparent inconsistencies in estimates of terrestrial CO_2 sources and sinks, Tellus B, 55, 345–363, 2003.

Hungershoefer, K., Breon, F.-M., Peylin, P., Chevallier, F., Rayner, P., Klonecki, A., Houweling, S., and Marshall, J.: Evaluation of various observing systems for the global monitoring of CO_2 surface fluxes, Atmos. Chem. Phys., 10, 10503–10520, doi:10.5194/acp-10-10503-2010, 2010.

IPCC: Summary for Policymakers. In Climate Change 2007: The Physical Science Basis. Contribution of Working Group I to the Fourth Assessment Report of the Intergovernmental Panel on Climate Chang, edited by: Solomon, S., Qin, D., Manning, M., Chen, Z., Marquis, M., Averyt, K. B., Tignor, M., and Miller, H. L., Cambridge University Press, Cambridge, UK and New York, NY, USA, 2007.

Jones, N., Griffith, D., Velazco, V., Macatangay, R., O'Brien, D., Clark, A., and Rayner, P.: SolarFTS-lite down under, in: IRWG/TCCON Meeting, Wengen, Switzerland, 11–15 June 2012, 2012.

Kobayashi, N., Inoue, G., Kawasaki, M., Yoshioka, H., Minomura, M., Murata, I., Nagahama, T., Matsumi, Y., Tanaka, T., Morino, I., and Ibuki, T.: Remotely operable compact instruments for measuring atmospheric CO_2 and CH_4 column densities at surface monitoring sites, Atmos. Meas. Tech., 3, 1103–1112, doi:10.5194/amt-3-1103-2010, 2010.

Kuze, A., Suto, H., Nakajima, M., and Hamazaki, T.: Thermal and near infrared sensor for carbon observation Fourier-transform spectrometer on the Greenhouse Gases Observing Satellite for greenhouse gases monitoring, Appl. Optics, 48, 6716–6733, 2009.

Lauvaux, T., Uliasz, M., Sarrat, C., Chevallier, F., Bousquet, P., Lac, C., Davis, K. J., Ciais, P., Denning, A. S., and Rayner, P. J.: Mesoscale inversion: first results from the CERES campaign with synthetic data, Atmos. Chem. Phys., 8, 3459–3471, doi:10.5194/acp-8-3459-2008, 2008.

Levy, J. I., Spengler, J. D., Hlinka, D., Sullivan, D., and Moon, D.: Using CALPUFF to evaluate the impacts of power plant emissions in Illinois: mode sensitivity and implications, Atmos. Environ., 36, 1063–1075, 2002.

Lin, Y. L., Farley, R. D., and Orville, H. D.: Bulk parameterization of the snow field in a cloud model, J. Appl. Meteorol., 22, 1065–1092, 1983.

Lindenmaier, R., Dubey, M. K., Henderson, B. G., Butterfield, Z. T., Herman, J. R., Rahn, T., and Lee, S.: Multiscale observations of CO_2, $^{13}CO_2$, and pollutants at Four Corners for emission verification and attribution, P. Natl. Acad. Sci. USA, 111, 8386–8391, doi:10.1073/pnas.1321883111, 2014.

Mahadevan, P., Wofsy, S. C., Matross, D. M., Xiao, X., Dunn, A. L., Lin, J. C., Gerbig, C., Munger, J. W., Chow, V. Y., and Gottlieb, E. W.: A satellite-based biosphere parameterization

for net ecosystem CO_2 exchange: Vegetation Photosynthesis and Respiration Model (VPRM), Global Biogeochem. Cy., 22, GB2005, doi:10.1029/2006GB002735, 2008.

Mlawer, E. J., Taubman, S. J., Brown, P. D., Iacono, M. J., and Clough, S. A.: Radiative transfer for inhomogeneous atmospheres: RRTM, a validated correlated-k model for the longwave, J. Geophys. Res.-Atmos., 102, 16663–16682, 1997.

Monin, A. S. and Obukhov, A. M.: Basic laws of turbulent mixing in the surface layer of the atmosphere, Geophysical Institute of the Slovak Academy of Sciences, 24, 163–187, 1954.

Nilsson, S., Jonas, M., Shvidenko, A., Stolbovoi, V., and McCallum, I.: Monitoring, verification and permanence of carbon sinks, Abstract from the CarboEurope Conference "The Continental Carbon Cycle", Lisbon, Portugal, 19–21 March 2003, CarboEurope, 2003.

Petri, C., Warneke, T., Jones, N., Ridder, T., Messerschmidt, J., Weinzierl, T., Geibel, M., and Notholt, J.: Remote sensing of CO_2 and CH_4 using solar absorption spectrometry with a low resolution spectrometer, Atmos. Meas. Tech., 5, 1627–1635, doi:10.5194/amt-5-1627-2012, 2012.

Peylin, P., Law, R. M., Gurney, K. R., Chevallier, F., Jacobson, A. R., Maki, T., Niwa, Y., Patra, P. K., Peters, W., Rayner, P. J., Rödenbeck, C., van der Laan-Luijkx, I. T., and Zhang, X.: Global atmospheric carbon budget: results from an ensemble of atmospheric CO_2 inversions, Biogeosciences, 10, 6699–6720, doi:10.5194/bg-10-6699-2013, 2013.

Rannik, U., Aubinet, M., Kurbanmuradov, O., Sabelfeld, K., Markkanen, T., and Vesala, T.: Footprint analysis for measurements over a heterogeneous forest, Bound.-Lay. Meteorol., 97, 137–166, 2000.

Rayner, P. J. and O'Brien, D. M.: The utility of remotely sensed CO_2 concentration data in surface source inversions, Geophys. Res. Lett., 28, 175–178, 2001.

Rayner, P. J., Enting, I. G., Francey, R. J., and Langenfelds, R.: Reconstructing the recent carbon cycle from atmospheric CO_2, $\delta^{13}C$ and O_2/N_2 observations, Tellus B, 51, 213–232, 1999.

Rayner, P. J., Law, R. M., Allison, C. E., Francey, R. J., Trudinger, C. M., and Pickett-Heaps, C.: Interannual variability of the global carbon cycle (1992–2005) inferred by inversion of atmospheric CO_2 and $^{13}CO_2$ measurements, Global Biogeochem. Cy., 22, GB3008, doi:10.1029/2007GB003068, 2008.

Rayner, P. J., Raupach, M. R., Paget, M., Peylin, P., and Koffi, E.: A new global gridded data set of CO_2 emissions from fossil fuel combustion: methodology and evaluation, J. Geophys. Res., 115, D19306, doi:10.1029/2009JD013439, 2010.

Rodgers, C. and Connor, B.: Intercomparison of remote sounding instruments, J. Geophys. Res., 108, 4116–4229, 2003.

Schuepp, P. H., Leclerc, M. Y., Macpherson. J. I., and Desjardins, R. L.: Footprint prediction of scalar fluxes from analytical solutions of the diffusion equation, Bound.-Lay. Meteorol., 50, 355–373, 1990.

Shindell, D. and Faluvegi, G.: The net climate impact of coal-fired power plant emissions, Atmos. Chem. Phys., 10, 3247–3260, doi:10.5194/acp-10-3247-2010, 2010.

Skamarock, W. C. and Klemp, J. B.: A time-split nonhydrostatic atmospheric model for weather research and forecasting applications, J. Comput. Phys., 227, 3465–3485, 2008.

~~Solomon, S., Qin, D., Manning, M., Chen, Z., Marquis, M., Averyt, K. B., Tignor, M., and Miller, H. L.: Climate Change 2007: The physical Science Basis, Contribution of Working Group I to the Fourth Assessment Report of the Intergovernmental Panel on Climate Change (IPPC), Cambridge University Press, The Pitt Building, Trumpington Street, Cambridge, UK, 996 pp., 2007.~~

Talbot, C., Bou-Zeid, E., and Smith, J.: Nested mesoscale large-eddy simulations with WRF: performance in real test cases, J. Hydrometeorol., 13, 1421–1441, 2012.

Toon, G. C., Blavier, J. F. L., Washenfelder, R. A., Wunch, D., Keppel-Aleks, G., Wennberg, P. O., Connor, B. J., Sherlock, V., Griffith, D. W. T., Deutscher, N. M., and Notholt, J.: Total Column Carbon Observing Network (TCCON), in: Fourier Transform Spectroscopy Vancouver Canada, 26–30 April, ISBN: 978-1-55752-871-1 FTS/HISE Joint Session (JMA) doi:10.1364/FTS.2009.JMA3, 2009.

Wunch, D., Toon, G. C., Wennberg, P. O., Wofsy, S. C., Stephens, B. B., Fischer, M. L., Uchino, O., Abshire, J. B., Bernath, P., Biraud, S. C., Blavier, J.-F. L., Boone, C., Bowman, K. P., Browell, E. V., Campos, T., Connor, B. J., Daube, B. C., Deutscher, N. M., Diao, M., Elkins, J. W., Gerbig, C., Gottlieb, E., Griffith, D. W. T., Hurst, D. F., Jiménez, R., Keppel-Aleks, G., Kort, E. A., Macatangay, R., Machida, T., Matsueda, H., Moore, F., Morino, I., Park, S., Robinson, J., Roehl, C. M., Sawa, Y., Sherlock, V., Sweeney, C., Tanaka, T., and Zondlo, M. A.: Calibration of the Total Carbon Column Observing Network using aircraft profile data, Atmos. Meas. Tech., 3, 1351–1362, doi:10.5194/amt-3-1351-2010, 2010.

Wunch, D., Wennberg, P. O., Toon, G. C., Connor, B. J., Fisher, B., Osterman, G. B., Frankenberg, C., Mandrake, L., O'Dell, C., Ahonen, P., Biraud, S. C., Castano, R., Cressie, N., Crisp, D., Deutscher, N. M., Eldering, A., Fisher, M. L., Griffith, D. W. T., Gunson, M., Heikkinen, P., Keppel-Aleks, G., Kyrö, E., Lindenmaier, R., Macatangay, R., Mendonca, J., Messerschmidt, J., Miller, C. E., Morino, I., Notholt, J., Oyafuso, F. A., Rettinger, M., Robinson, J., Roehl, C. M., Salawitch, R. J., Sherlock, V., Strong, K., Sussmann, R., Tanaka, T., Thompson, D. R., Uchino, O.,

Warneke, T., and Wofsy, S. C.: A method for evaluating bias in global measurements of CO_2 total columns from space, Atmos. Chem. Phys., 11, 12317–12337, doi:10.5194/acp-11-12317-2011, 2011a.

Wunch, D., Toon, G. C., Blavier, J. L., Washenfelder, R., Notholt, J., Connor, B. J., Griffith, D. W. T., Sherlock, V., and Wennberg, P. O.: The Total Carbon Column Observing Network, Philos. T. R. Soc. A, 369, 2087–2112, doi:10.1098/rsta.2010.0240, 2011b.

Table 1. Physics schemes used in WRF model set-up for Port Augusta.

Type	Selected Option	References
Boundary Layer	YSU scheme	Hong et al. (2006)
Land surface	NOAH land-surface model	Chen and Dudhia (2001)
Surface layer	Monin–Obukhov (Janjic Eta) scheme	Monin and Obukhov (1954)
Long-wave radiation	Rapid Radiative Transfer scheme	Mlawer et al. (1997)
Short-wave radiation	Goddard shortwave scheme	Chou and Suarez (1994)
Microphysics	WRF single-moment 5-class scheme (Lin)	Lin et al. (2003)
Cumulus scheme	Grell 3-D ensemble scheme	Grell and Dèvènyi (2002)

Table 2. Multiplication factors, uncertainties, root-mean-square error (RMSE) of model-data mismatches and correlation (source + background and source only), from optimisation of measured and simulated in-situ and column-averaged CO_2.

Case	Multiplier	Uncertainty	RMSE	Corr (S + B)	Corr (S)
WRF-surface	0.12	0.05	0.78	0.30	0.42
WRF column	1.06	0.54	0.44	0.72	0.67

Table 3. Multiplication factors, uncertainties and root-mean-square error (RMSE) of model-data mismatches from optimisation of measured and simulated X_{CO_2} tracer for various emission scenarios.

Case	Emission factor	Uncertainty	RMSE	Corr $(S + B)$	Corr (S)
L5	1.06	0.54	0.43	0.72	0.68
L6	1.05	0.54	0.44	0.72	0.67
L7	1.00	0.55	0.46	0.68	0.63
PR	1.00	0.55	0.45	0.69	0.64

Table 4. Multiplication factors, uncertainties and root-mean-square error (RMSE) of model-data mismatches from optimisation of measured and simulated X_{CO_2} tracer for model data sampled every 5, 10, and 20 min.

Sample time (min)	Emission factor	Uncertainty	RMSE	Corr (S + B)	Corr (S)	Sample size
5	1.05	0.54	0.44	0.72	0.67	24
10	0.99	0.56	0.45	0.70	0.63	23
20	0.80	0.61	0.42	0.64	0.58	20

Table 5. Multiplication factors, uncertainties and root-mean-square error (RMSE) of model-data mismatches from optimisation of measured and simulated X_{CO_2} tracer for model run with diurnally varying and constant emissions.

Case	Emission factor	Uncertainty	RMSE	Corr $(S + B)$	Corr (S)
AEMO (diurnal)	1.05	0.54	0.44	0.72	0.67
Constant	1.32	0.60	0.41	0.78	0.74
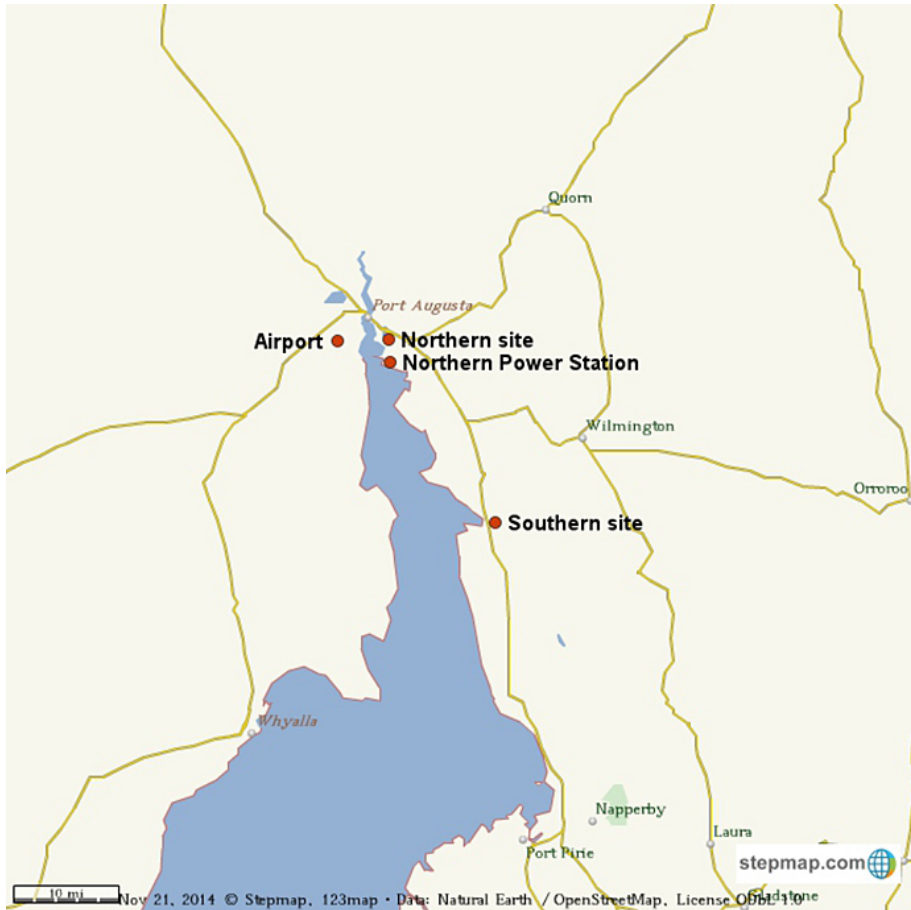
Figure 1. Map of Port Augusta showing locations of the Northern and Southern sites, Northern Power Station, Airport, Spencer Gulf (blue water feature) and nearby towns. The Southern site is located at Miranda, with Stirling North about 2km directly east of the Northern site
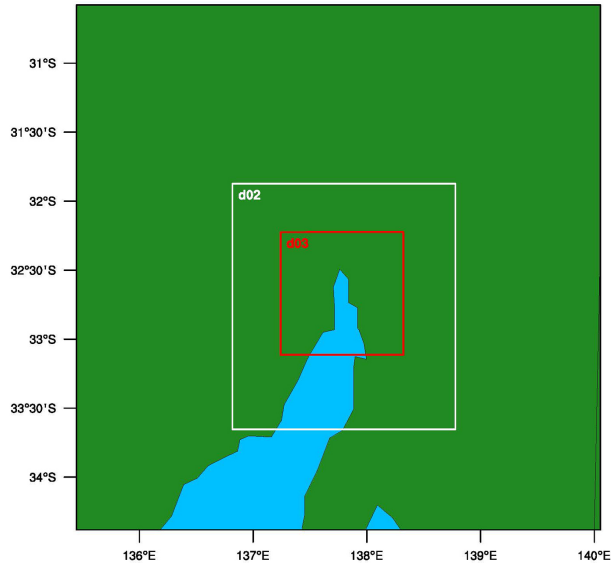
Figure 2. Map showing three-nested domains used for modelling CO_2 at Port Augusta. Grid resolutions are 9, 3 km, and 1 km for the outermost, intermediate and innermost domains, respectively
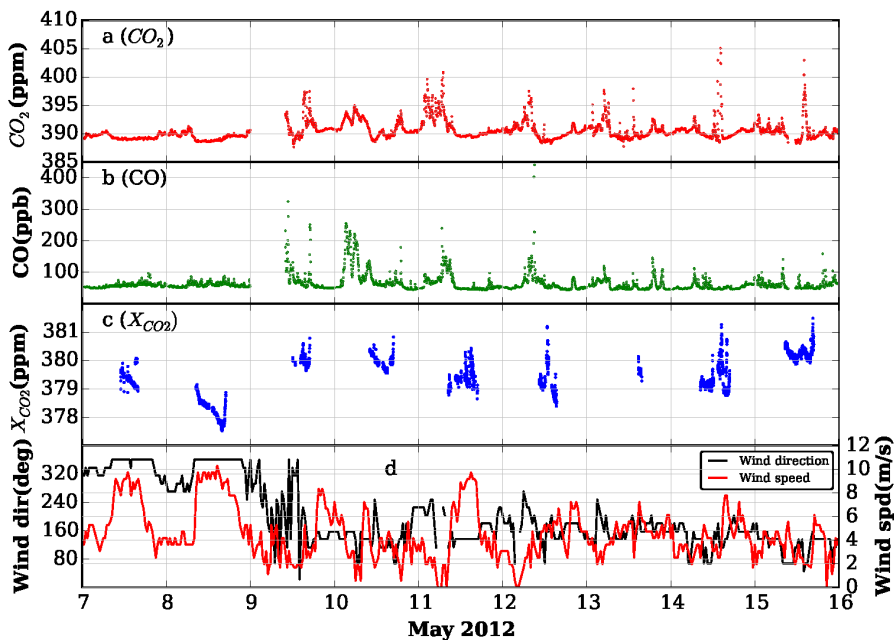
Figure 3. Measured time series of in-situ concentrations of CO_2 **(a)** and CO **(b)**, column-averaged X_{CO_2} **(c)** and wind direction and wind speed **(d)**. The concentrations were measured at the Northern site 3 km north of the NPS.
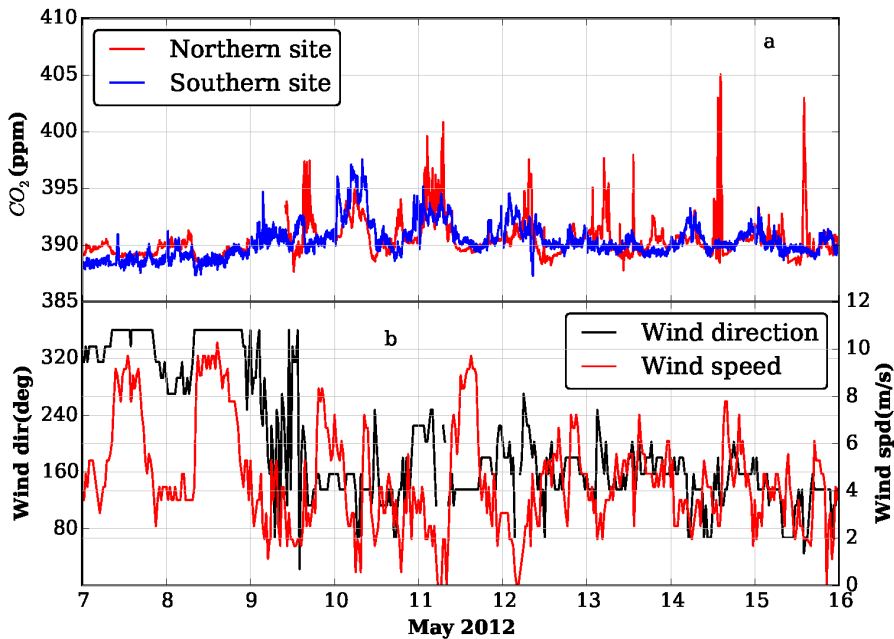
Figure 4. Time-series of in situ CO_2 concentrations measured at the Northern and Southern sites **(a)** as well as wind direction and wind speed **(b)** measured at Port Augusta airport.
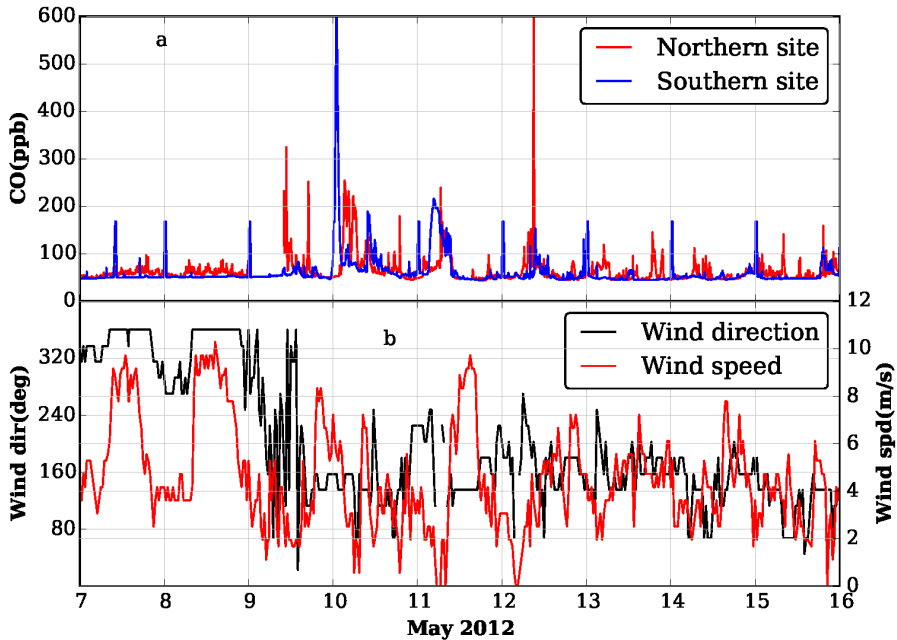
Figure 5. Time-series of in-situ CO concentrations measured at the Northern and Southern sites **(a)** as well as wind direction and speed **(b)** measured at Port Augusta airport.
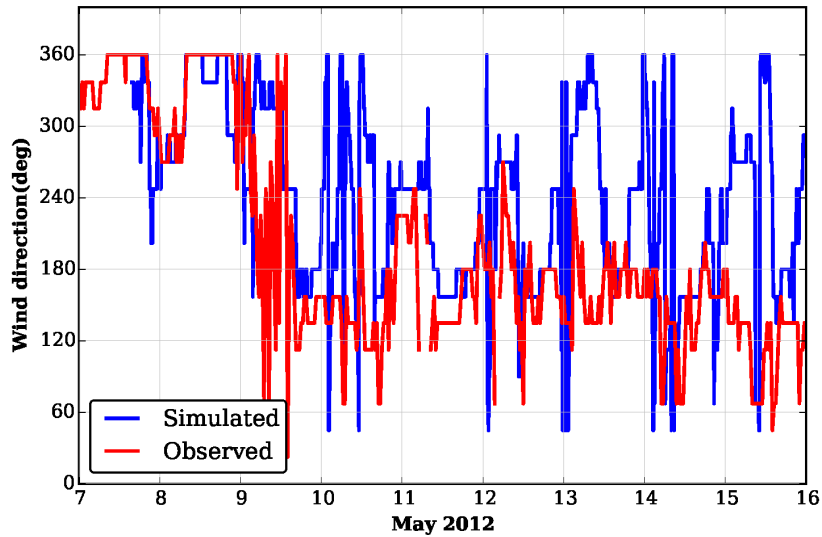
Figure 6. Comparison of simulated and observed wind direction for Port Augusta airport.
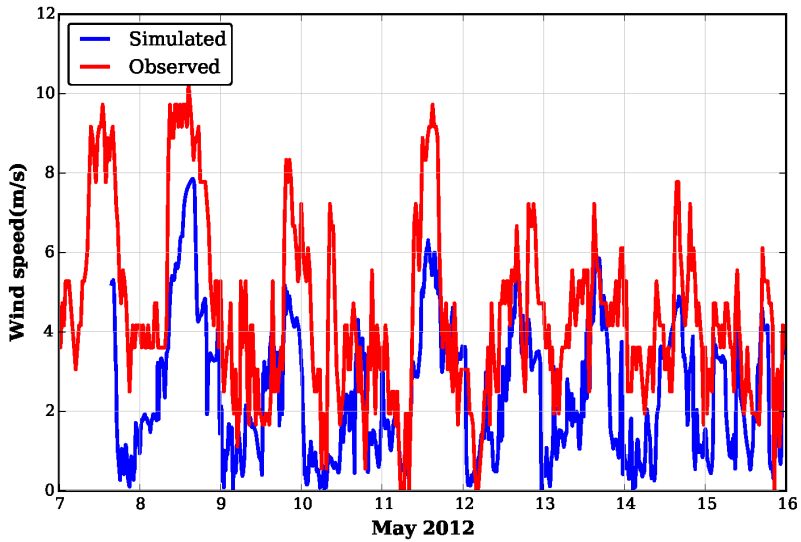
Figure 7. Comparison of simulated and observed wind speed for Port Augusta airport.
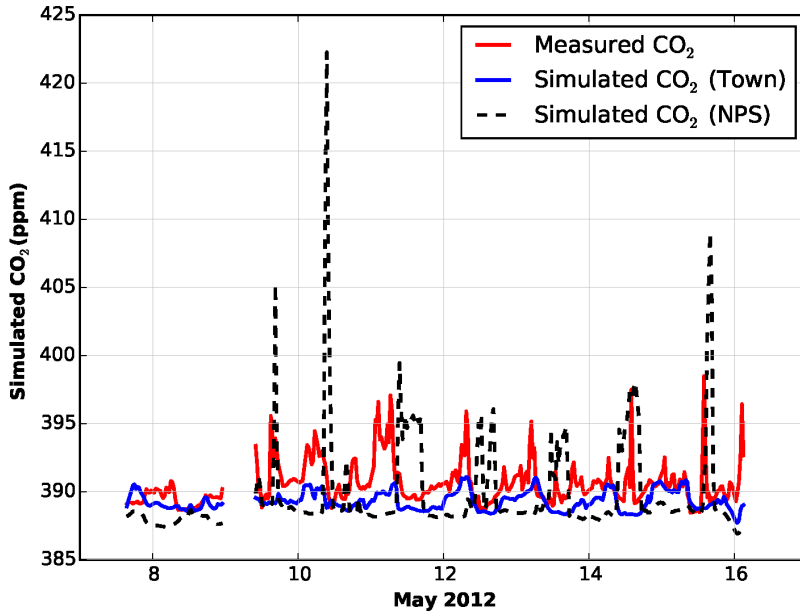
Figure 8. Measured and modelled time series of in-situ CO_2. Two independent tracers are simulated, one from the NPS and the other from Port Augusta (Town)
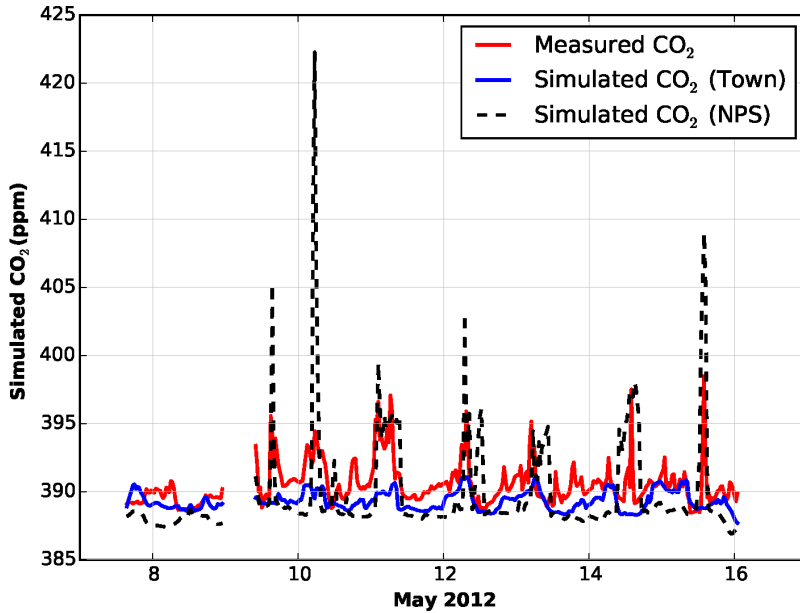
Figure 9. Measured and modelled time series of in-situ night-time and daytime CO_2 concentrations, with some peaks matched in time to account for sea breeze and recirculation.

(a) 8 May 2012

(b) 10 May 2012

(c) 11 May 2012

(d) 14 May 2012
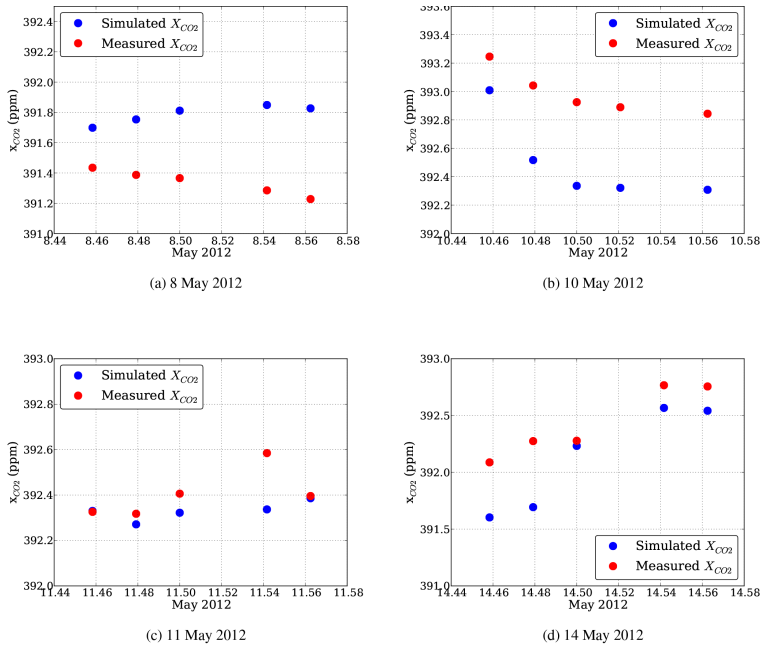
Figure 10. Time-series of measured and simulated X_{CO_2} (from the NPS tracer) for selected days.

47
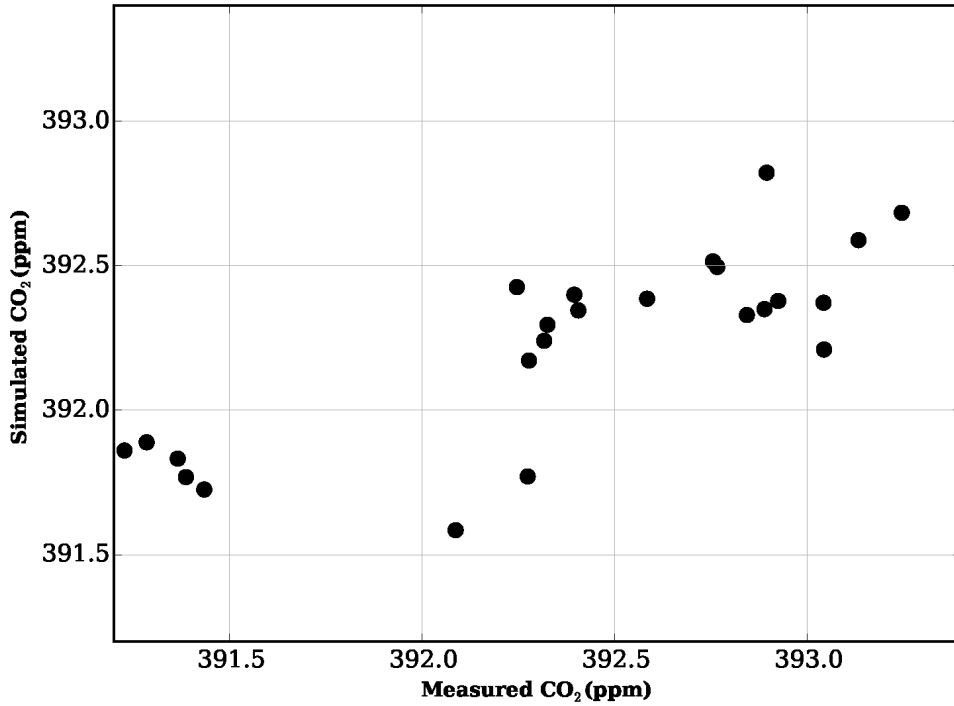
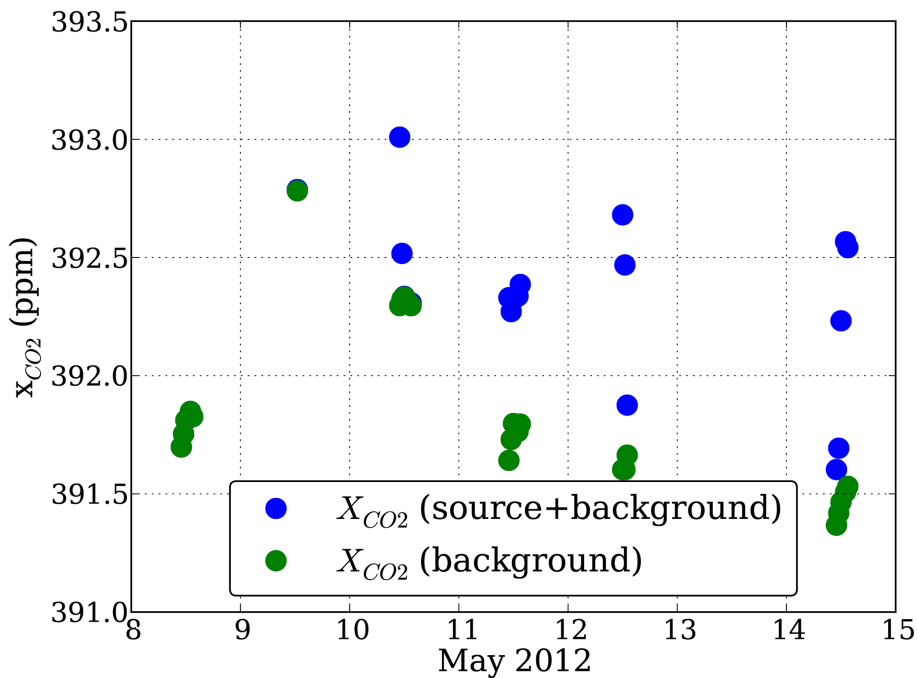**Figure 11.** Scatter plot of measured vs. simulated X_{CO_2}.

Figure 12. Half-hourly averaged time-series of modelled X_{CO_2} concentrations for the power plant source + MACC CO_2 background tracer and the tracer with MACC CO_2 background only.
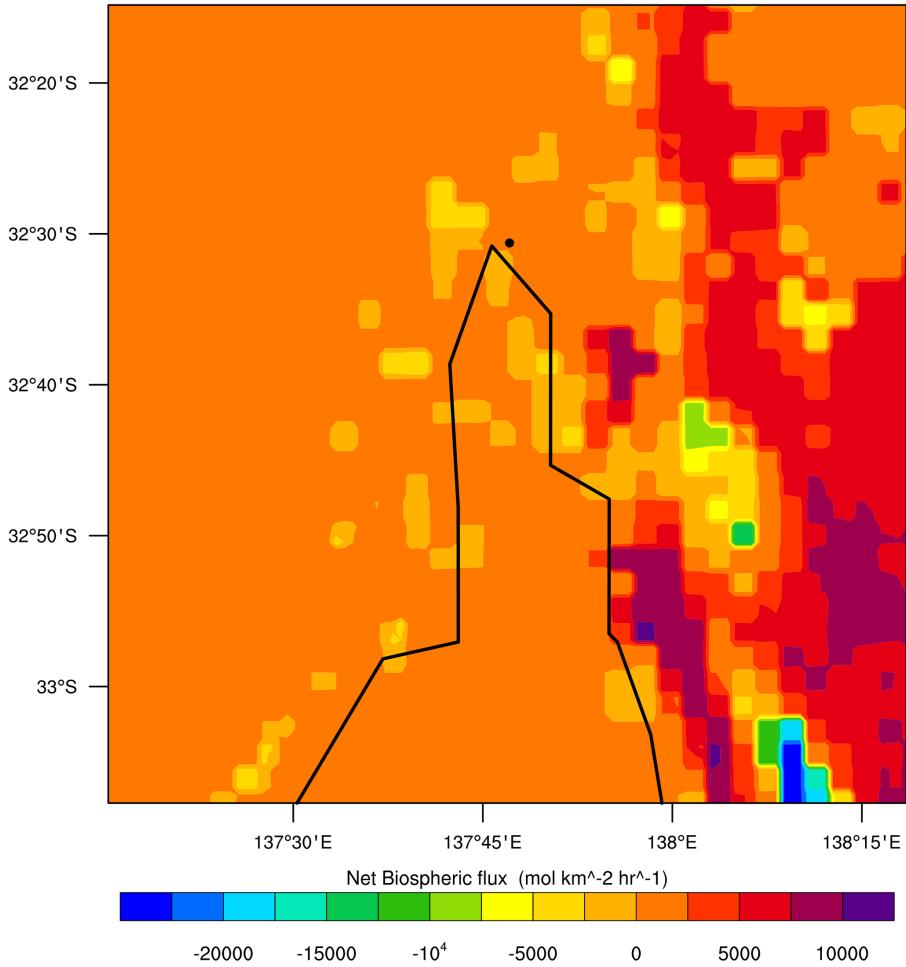
Net Biospheric flux (mol km^-2 hr^-1)

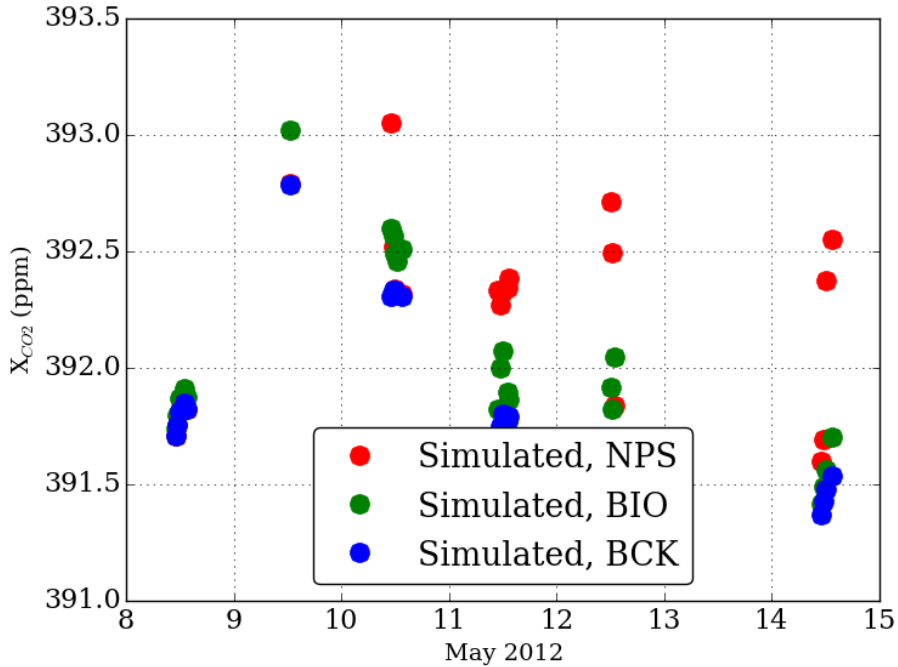**Figure 13.** Map of net biospheric fluxes in Port Augusta as generated by WRF-VPRM for 13 May 2012 and 10.00 a.m.

Figure 14. Simulated NPS tracer, biospheric tracer (BIO) and background MACC CO_2 tracer (BCK).